ELSEVIER

Low energy response calibration of the BATSE large area detectors onboard the Compton Observatory

C.E. Laird[a],*, B.A. Harmon[b], Colleen A. Wilson[b], David Hunter[a], Jason Isaacs[a]

[a]Department of Physics and Astronomy, Eastern Kentucky University, Moore 351, 521 Lancaster Avenue, Richmond, KY 40475-3124, USA
[b]XD12 NASA/Marshall Space Flight Center, Huntsville, AL 35812, USA

Abstract

The low-energy attenuation of the covering material of the Burst and Transient Source Experiment (BATSE) large area detectors (LADs) on the Compton Gamma Ray Observatory as well as the small-angle response of the LADs have been studied. These effects are shown to be more significant than previously assumed. The LAD entrance window included layers of an aluminum-epoxy composite (hexel) that acted as a collimator for the lowest energy photons entering the detector just above threshold (20–50 keV). Simplifying assumptions made concerning the entrance window materials and the angular response at incident angles near normal to the detector face in the original BATSE response matrix formalism had little effect on γ-ray burst measurements; however, these assumptions created serious errors in measured fluxes of galactic sources, whose emission is strongest near the LAD energy threshold. Careful measurements of the angular and low-energy dependence of the attenuation due to the hexel plates only partially improved the response. A systematic study of Crab Nebula spectra showed the need for additional corrections: an angular-dependent correction for all detectors and an angular-independent correction for each detector. These corrections have been applied as part of an overall energy and angular-dependent correction to the BATSE response matrices.

1. Introduction

The observation of X-rays and γ rays by detector systems in Earth orbit is one of the more useful tools in the study of the energetic processes occurring throughout the Universe. Phenomena such as γ-ray bursts (GRBs) were not seen before the orbiting of γ-ray detectors. GRBs, first reported in 1972, were observed by the Air Force VELA satellites [1], yet their origin remained a mystery until combined X-ray, γ-ray and optical observations revealed that most GRBs are at cosmological distances [2].

The Burst and Transient Source Experiment (BATSE) aboard the Compton Gamma Ray Observatory (CGRO) [3] was designed to detect and map the energy, temporal and sky distributions of GRBs. Of the four experiments onboard CGRO, BATSE covered the lowest γ-ray energies ($>\sim$10 keV–2 MeV) and consisted of eight detector modules mounted in an octahedral geometry to allow a full 4π view of the sky. As shown in Fig. 1, each module contained a large area detector (LAD) consisting of a 1.27-cm ($\frac{1}{2}$-in.) thick, 50.8-cm (20-in.) diameter NaI crystal with light collector and photomultiplier tubes located behind a charged particle detector (CPD) and covered with multi-layer insulation material for thermal control in low Earth orbit [4]. The CPD, made of a 6.35-mm ($\frac{1}{4}$-in.) plastic scintillator (polystyrene), acted as a "veto" detector rejecting signals produced by incident charged particles. The CPD was supported between 6.35-mm thick aluminum plates consisting of two 254-μm (10-mil) outer aluminum sheets held together by an aluminum-epoxy structure, known as "hexel". The honeycomb-like hexel consisted of

*Corresponding author. Tel.: +1 859 622 1526; fax: +1 859 622 1399.
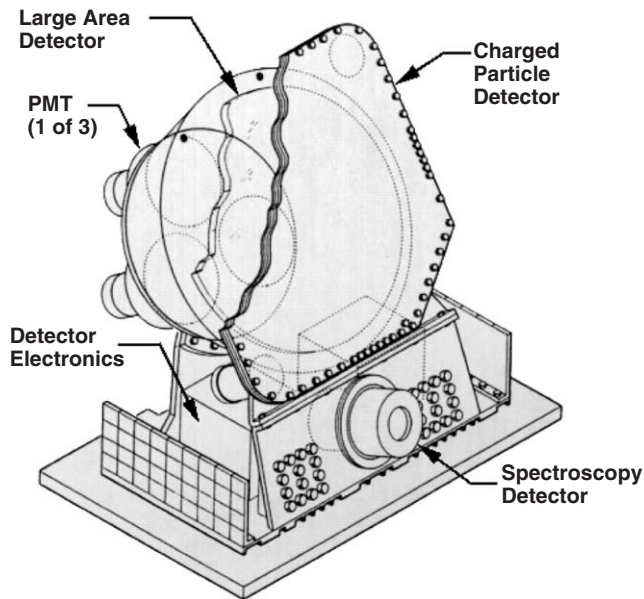E-mail address: Chris.Laird@eku.edu (C.E. Laird).

Fig. 1. A diagram of a BATSE detector module. The large area detector (LAD) is actively shielded by a multi-layer entrance window consisting of a charged particle, plastic scintillator detector (CPD) supported between two hexel aluminum plates.

small, non-uniform six-sided cells of roughly $\sim\frac{1}{3}-\frac{2}{3}$ mm ($\frac{1}{8}-\frac{1}{4}$ in.) characteristic width and non-uniform cross-section, oriented such that cell walls were nearly perpendicular to the LAD entrance window to minimize absorption of incident photons.

The LAD response was carefully calibrated between $\sim$50 keV and $\sim$2 MeV at several incident angles using standard γ-ray sources before launch [4]. These calibrations were then compared to a Monte Carlo model of the entire system to assure a complete understanding of the effects of scattering and absorption from the cover material, nearby components, and the Earth's atmosphere. The model gave good agreement to the measured detector response, and was used to reduce observed signals into absolute fluxes and to provide sky locations for the GRBs [5]. For on-orbit measurements of GRBs, where the incident angle was determined by fitting the response to the observed signal, a third degree polynomial in the cosine of the incident angle was used to interpolate and provide a smooth transition between model response matrices generated at a selected set of angles between $0°$ and $90°$ [4].

Photons detected by the NaI detectors were initially analyzed onboard the spacecraft in several ways. One way was to count the photon signal in ranges of energies or channels as would be done with single channel analyzers. The ranges of the energy channels were set before launch and were designed to measure in increasing energy ranges from about 20 keV to about 2 MeV so that there would be 16 channels of data [6]. Channel 0 was about 12–20 keV, channel 1, 20–30 keV, and channel 2, 30–40 keV, etc., with wider band-passes at higher energy. Barring changes brought on from launching the spacecraft, or from temperature or other stresses in orbit, the eight detectors

should have the same response, after correcting for effects of different angles of incidence, to any external γ-ray or X-ray source.

The success of the initial LAD response calibration [4] was in part dependent on the spectral behavior of GRBs, which generally has the largest contribution to the total luminosity well above the LAD energy threshold. This means that the deposited energy per channel can increase for a GRB above threshold up to some break energy, typically $\sim$0.2 MeV. On the other hand, most non-GRB astronomical sources detected with the LADs exhibit power law or thermal-like spectra with photon indices usually between -2 and -4, or a kT of 30–120 keV. Thus, at 20 keV (channel 1), the energy flux of many non-burst sources could be 10 times the flux at 50 keV. It was found that serious errors in the total fluence could result from neglecting the low-energy range of the LADs ($\sim$20–60 keV) in fitting spectral models to data. In such instances, careful determination of the detector system response in the 20–60 keV range was important to BATSE measurements of sources other than GRBs.

Questions on the accuracy of the pre-launch LAD response calibration for all eight detectors came from measurements of the radiation from the Crab Nebula using Earth occultation and pulsed timing techniques [5,7]. Earth occultation measurements of the Crab provided the most convenient and useful tool for investigating the near threshold response of the LADs. The Crab Nebula has a well studied, and for present application, constant γ-ray spectrum. Using the Earth occultation technique [7], Crab data were collected over a period of about 5 years in all eight LADs in all energy bins and at different aspect angles (θ) measured with respect to the normal to the surface of the LAD (Fig. 1) and otherwise independent of direction. This was made possible by the repointing of the CGRO, which nominally occurred about every 2 weeks, for the benefit of observers using the on-board telescopes. These data were organized into angular distributions for each energy channel in all eight LADs. The solid circles with error bars in Fig. 2 show the Crab data set for all LADs, channel 1 (20–30 keV) along with the predicted response shown by the continuous curve [7]. The predicted responses were made using the initial LAD calibration [4] convoluted with the Crab spectrum published by Jung [8]. The angular distribution data for all detectors exhibited a very prominent forward-angle peaked behavior that was different from the expected LAD response. The net effect on measured fluxes for all sources following deconvolution of the model response, was that whenever the direction to the source was near normal to the detector face, the inferred flux was considerably higher (30% or more) from that detector. The effect was particularly pronounced in the lowest energy channels just above threshold. However, use of the Crab Nebula as a "standard candle", and the fact that the LADs were gain-stabilized during the mission, provided a highly reproducible data set with which to investigate this effect.
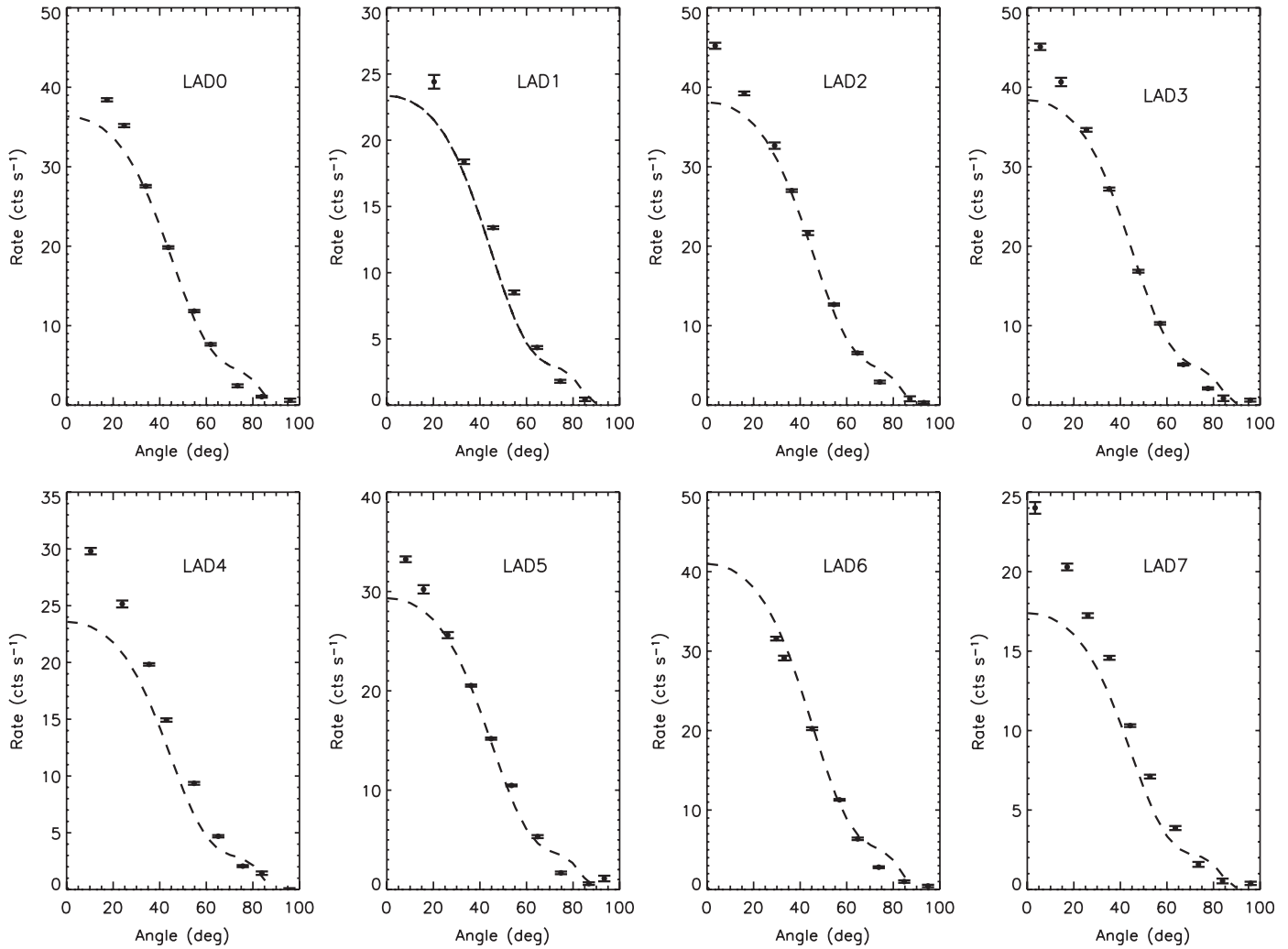
Fig. 2. Angular distribution of Crab Nebula Radiation for channel 1 of all LADs from Ref. [7]. The measured data with error bars are shown as well as the original detector response (dashed line).

2. Experimental measurements

To better understand why use of the original detector response did not properly predict the actual Crab Nebula measurements at small angles and near threshold, a direct measurement of the attenuation effects of the material covering the NaI crystals was performed. The primary absorbing components of the LAD entrance window were the plastic scintillator (CPD) used to detect charged particles, and the two layers of hexel. The CPD and supporting layers of hexel covered the entire front face of the NaI detector as shown in the cutaway view in Fig 1. Samples of these materials were obtained from the NASA/ Marshall Space Flight Center for attenuation measurements at the Nuclear Physics Laboratory at Eastern Kentucky University (EKU). The CPD (and hexel plate) is octagonal with 22-cm (23.3-cm) sides modified into irregular hexagons by adding additional material until two sides enclosed a third. The wings of the CPD allowed it to be coupled with a photomultiplier tube (PMT; see dotted-circle at the top of Fig. 1). The wings of the hexel plates

were solid except for circular cutouts for mounting the PMTs and tapped holes for mounting screws. The edge of the hexel plate was also solid to a width of about 6.3 mm. There were numerous holes in the solid aluminum so that it could be attached to other structure on the spacecraft. The thicknesses of the hexel plate and the CPD were measured with a micrometer at several points on the surface and found to be 7.14 ± 0.08 and 6.35 ± 0.10 mm compared with the reported values of 7 and 6.35 mm, respectively [9].

Fig. 3 shows three different views of the experimental arrangement used for photon attenuation measurements. The sample material (the hexel is indicated here), source, and a thin window 5.08×5.08-cm NaI detector were placed on the z-axis. The samples were mounted on an optical spectrometer base modified especially for these measurements. θ gives the angle from the source to the normal to the absorbing material, while ϕ represents a rotation about the normal. The spectrometer scale was used to determine accurately the angle of incidence of the photons. The alignment of the system was established with a laser in such a manner that the axis of the detector was
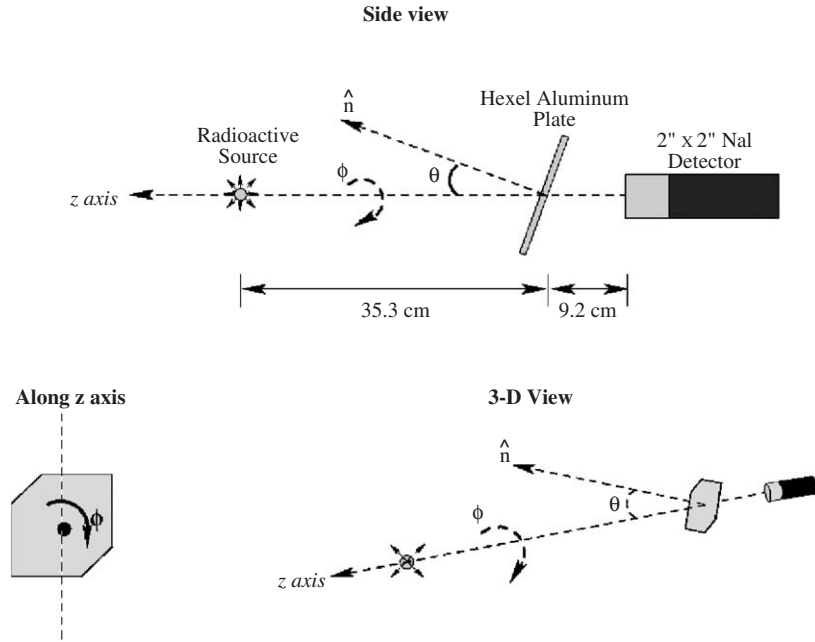
Side view

Along z axis   **3-D View**

Fig. 3. Three views of the experimental arrangement used to measure the transmission through the LAD components. As shown, θ is the angle of incidence from the source to the plate and φ is the angle of rotation about the normal or z-axis when $\theta = 0$.

aligned with the radioactive source and perpendicular to the absorbing material. This insured that, for $\theta = 0°$, the center of the absorbing material would be perpendicular to the laser beam as well as the photons from the radioactive sources. Photons with energies of 14.4 keV (Co-57), 22.6 keV (Cd-109), 32.9 keV (Cs-137), and 59.9 keV (Am-241) were used to determine the ratio of the yield, with no absorber, to the yield with the absorber. These energies were selected to cover the range where the attenuation was expected to be almost total, up to energies where the original measurements of the detector response [4] were most likely valid. The NaI/PMT detector signal was amplified and analyzed with a Tennelec PCA multichannel analyzer connected to a desktop computer. Analysis windows were placed over the proper region of integration for a spectrum with no attenuator. Count rates above the continuum with and without absorber were used to measure relative transmission. Transmission measurements were made at each photon energy of interest at 5° increments of θ from normal incidence to about 60°, which is the largest acceptable angle allowed for analysis of BATSE data. The optimum source-to-absorber distance was increased until the transmission became a constant indicating that source-to-detector solid angle effects were insignificant.

Fig. 4 shows the transmission of a solid, flat aluminum plate of similar thickness (0.762 mm) to the hexel plate for angles from $-60°$ to $+60°$ for 22.6 keV photons (Cd-109) measured at various incident angles. The solid curve represents the transmission (T) calculated with
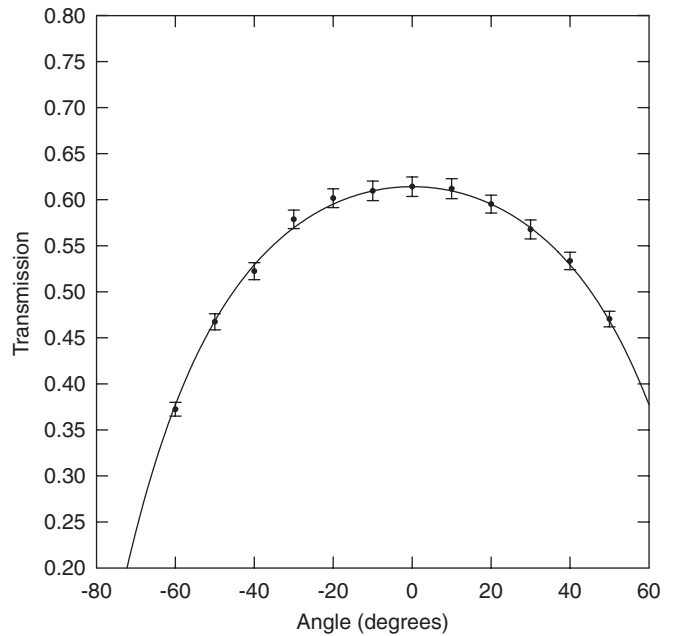
$$T = \exp(-\mu\rho t / \cos\theta) \qquad (1)$$

Fig. 4. The measured angular transmission (solid circles with error bars) of a solid aluminum plate with an area density similar to the hexel aluminum plates. The solid line shows the expected angular dependence of the transmission.

where θ is the incident angle, μ is the mass absorption coefficient [10], ρ is the density of the material, and t is the thickness of the plate. The mass absorption coefficient μ and the areal density ρt, found by weight and area measurement of the plate, were used to calculate the value of T for comparison to data. This measurement confirms
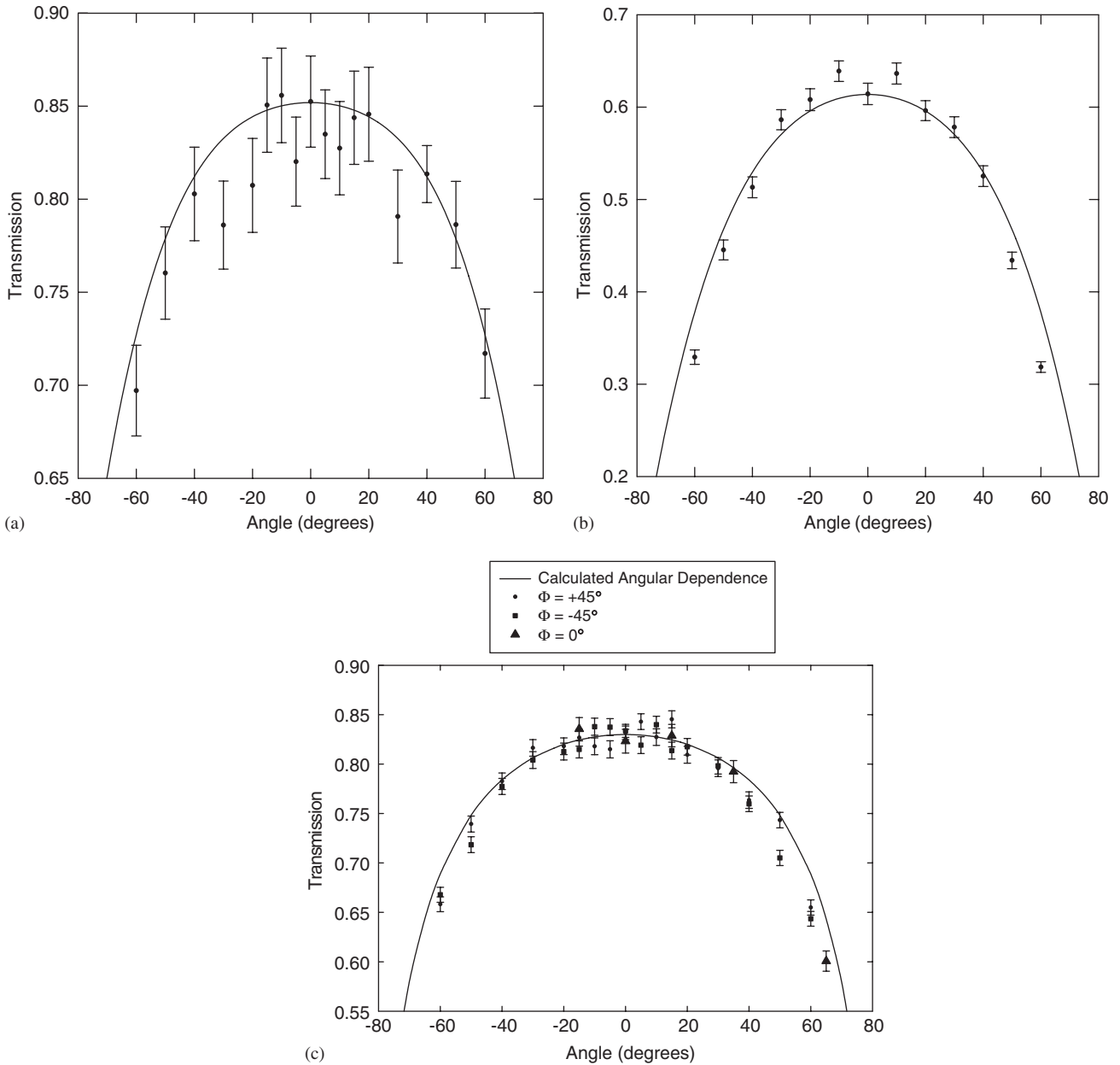
Fig. 5. (a) The measured angular transmission of the solid charge-particle detector (CPD) at 32.9 keV, (b) 14.4 keV, and (c) 22.6 keV. In each figure, the solid line shows the expected angular dependence of the transmission. Figure (c) shows data obtained at $(0°, \pm45°)$ angles of rotation φ about the incident photon (or z) axis. Although no intrinsic φ dependence was expected, this provided a check on the laser alignment procedure.

that the experimental arrangement effectively measures the transmission without solid-angle effect. The error bars are the propagated errors involving both the non-attenuated and the attenuated count rates.

To determine an accurate areal density (thickness) of the hexel plate and, for comparison, of the CPD normal-incident transmission measurements for 22.6 keV photons were made at a 135 points on the hexel plate, and several points on the uniform CPD disk. Using the mass absorption coefficient in Table 2 the weighted average of the areal density for the CPD was determined to be $0.667 \pm 0.005\,\mathrm{g/cm^2}$ which agrees well with the value $0.655\,\mathrm{g/cm^2}$ used in the original BATSE response matrix

[9]. For the hexel plate transmission, the plate was moved $0.5\,\mathrm{cm}$ horizontally for nine points and $1.0\,\mathrm{cm}$ vertically on an $8\,\mathrm{cm} \times 8\,\mathrm{cm}$ grid. Using the mass absorption coefficient in Table 2 the weighted-average areal density was determined to be $0.209 \pm 0.001\,\mathrm{g/cm^2}$ compared to $0.23\,\mathrm{g/cm^2}$ in the BATSE response matrix [9].

Figs. 5(a)–(c) show the transmission through the CPD as a function of incident angle (θ) for photon energies of 32.9, 14.4 and 22.6 keV, respectively. The attenuation for the CPD at 60 keV was sufficiently small ($\sim$12%) that measurements were not deemed necessary. Measurements at 22.6 keV (Fig. 5(c)) were performed at three angles ($\varphi = 0°, \pm45°$) about the z-axis and various incident angles

Table 1
Photon transmission through polystyrene CPD

Energy (keV)	Mass absorption coefficient (cm^2/g) [10]	Calculated transmission using $\rho t = 0.667$ g/cm^2	Measured transmission
14.4	0.8	0.585	0.614 ± 0.010
22.61	0.3	0.818	$0.832 \pm .007$
32.9	0.25	0.846	0.852 ± 0.025
59.9	0.19	0.88	Not measured

(θ) to confirm alignment of the experimental setup. As expected, the CPD data show that this material acts as a solid, uniform absorber at these photon energies. The normal incidence transmission obtained from the measured angular distributions at 14.4, 22.6 and 32.9 keV through the CPD is compared in Table 1 to the transmission calculated using $\mu(E)$ for polystyrene from the literature [10] and the areal density by direct weight and area measurements of the sample. The experimentally determined transmission at the three energies was within 1–3 sigma of the expected value.

Figs. 6(a)–(d) show the transmission through the hexel aluminum for various incident angles (θ) at photon energies of 14.4, 22.6, 32.9 and 59.9 keV, respectively. As was done for the CPD, measurements at 22.6 keV (Fig. 6(b)) were performed at three angles ($\varphi = 0°$, $\pm 45°$) about the z-axis. A check on possible solid-angle effects was performed by doubling the source to absorber distance at 22.6 keV, which yielded virtually identical results.

It can be seen in Figs. 6(a)–(c) that the deviation of the transmission from a solid, uniformly absorbing sheet as a function of the angle of incidence is very pronounced at the lower energies. In fact, the shape of the angular distribution at the lowest energy (14.4 keV) approaches the linear response seen in the LAD, preferentially allowing the highest transmission for normally incident photons. Photons entering at larger incident angles encounter much more material due to the multi-celled structure of the hexel. At 14.4 keV (Fig. 6(a)), the aluminum plate attenuates more than 80% of the normal-incident photons decreasing to about 15% at 32.9 keV (Fig. 6(c)).

In Table 2, we compare the normal-incidence transmission for the hexel sample obtained from the measured angular distributions at all four energies to the transmission calculated using $\mu(E)$ for aluminum from the literature [10] and the weighted-average areal density. The experimentally determined transmission at each of the four energies was within 1–2 sigma of the expected value.

From the data shown in Fig. 6(b), we calculated the effective thickness of the hexel as a function of angle of incidence using

$$T_{\text{measured}} = \exp(-\mu(E)\rho t_{\text{eff}}). \qquad (2)$$

The ρt_{eff} calculated for the hexel in 5° increments is given in Table 3. Fig. 6(c) shows the transmission of the 32.9 keV photons (shown by the diamonds and solid line) calculated with the effective thicknesses listed in Table 3 and the

known mass absorption coefficient, $\mu(E)$. To obtain a quality of fit we defined a χ^2 per degree of freedom (χ^2/N) of the form

$$\chi^2/N = \sum (T_{\text{measured}} - T_{\text{calculated}})^2 / N\sigma^2 \qquad (3)$$

where T_{measured} is the measured transmission through the hexel plate, $T_{\text{calculated}}$ is the transmission calculated with the effective thicknesses from the 22.6 keV data, σ is the statistical error in the transmission measurement, and N is the number of data points.

With this definition the χ^2 per degree of freedom was found to be 0.7. Thus, there is an excellent agreement between measured and calculated transmission at 32.9 keV for these 17 points.

We have used the attenuation measurements of the hexel and CPD in developing a model correction to the BATSE LAD response matrix formalism, which, in its original form [4], did not account for the collimating effect of hexel layers built into the LAD entrance window. We later concluded that this correction to the LAD response matrix was not adequate to provide a good predictor of the measured distribution of the Crab as a standard candle. An additional correction is discussed in the next section.

3. Model correction to BATSE response matrices

The BATSE response matrices were derived from Monte Carlo simulations of photons interacting with the detector modules (Fig. 1) and, to a limited degree, the surrounding mass of the spacecraft [4]. Simplifications in the geometry/ treatment were made, primarily to allow the tracing of many thousands of incident photons as they interacted with the materials making up the detectors and spacecraft in a finite period of time. These events, which involve Compton scatter, pair production, and photoelectric absorption, were binned at various angles and energies as they were absorbed in the material. For each hexel layer, an effective thickness of 0.23 mg/cm^2 was assumed in the original response model [9], as well as an assumption that the hexel was a uniform absorbing layer. Clearly, the experiment here shows that the latter was not a good assumption, as originally implied from observations of the Crab Nebula (Fig. 2) using the occultation technique.

Rather than repeat extensive simulations of the BATSE LAD matrices with a more sophisticated geometric representation of the entrance window, our approach was
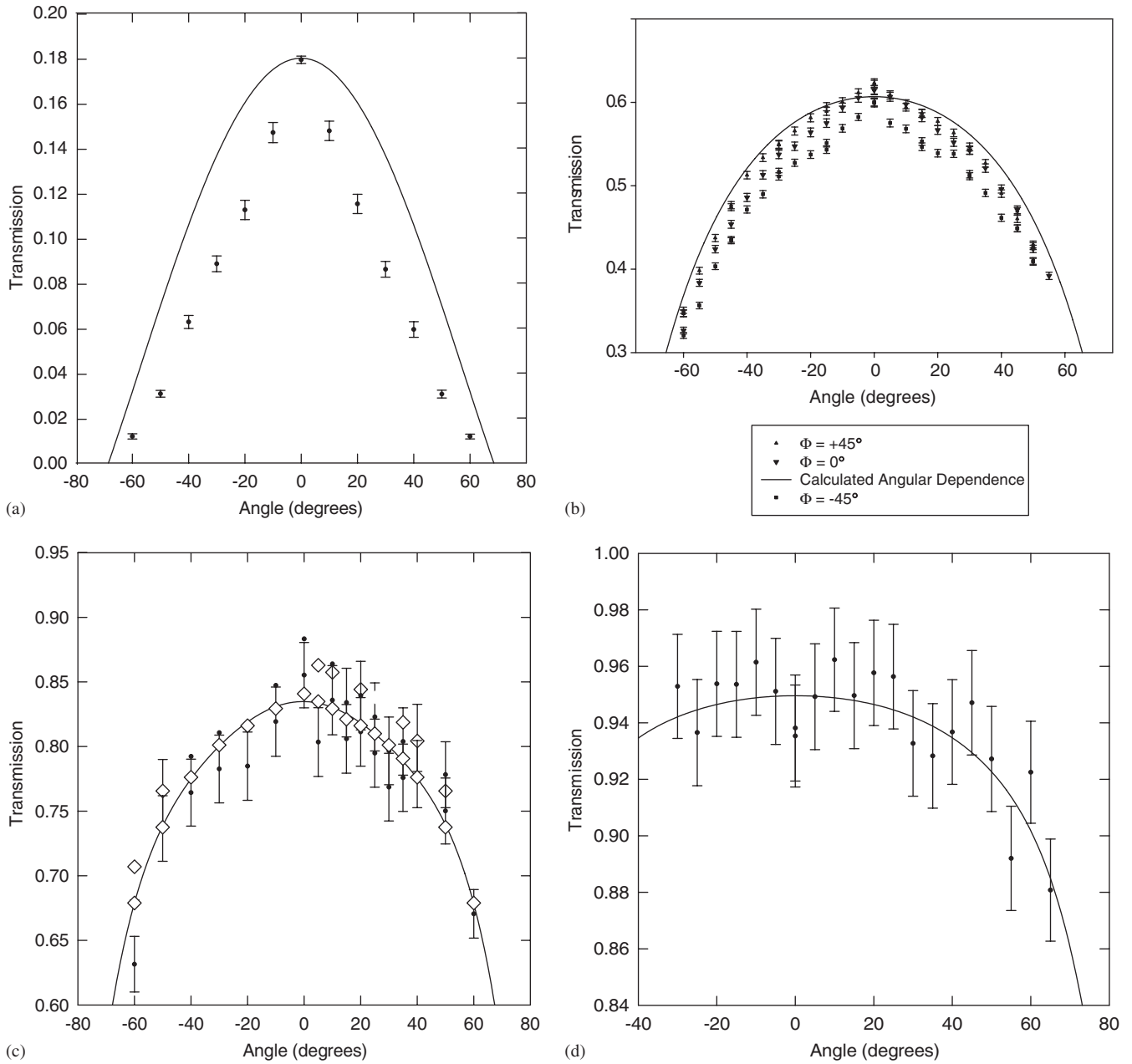
Fig. 6. (a) The measured angular transmission of the Hexel-aluminum plate at 14.4 keV, (b) 22.6 keV, (c) 32.9 keV, and (d) 59.9 keV. In each figure, the solid line shows the expected angular dependence of the transmission for a uniform aluminum plate of equivalent thickness, with the exception of (c), where the mass absorption coefficients from Table 2 and the effective thicknesses from Table 3 are used. As was done for the CPD, measurements at 22.6 keV ((b)) were performed at three angles ($\varphi = 0°$, $\pm 45°$) about the z-axis.

Table 2
Photon transmission through hexel aluminum plate

Energy (keV)	Mass absorption coefficient (cm²/g) [10]	Calculated transmission using $\rho t = 0.209 \, \text{g/cm}^2$	Measured transmission
14.4	8.3	0.177	0.179±0.002
22.6	2.39	0.607	0.610±0.020
32.9	0.84	0.84	0.809±0.023
59.9	0.28	0.94	0.935±0.018

to develop a multiplicative correction to the response matrices that would model the collimator-like transmission. The correction, applied directly to the matrices, over all input energies and incident angles, resulted in a new set of matrices that can be used in fitting the raw counts for the Crab Nebula as a function of energy channel.

Thus, before any spectral fitting, the input energy side of the BATSE detector response matrix was multiplied by a correction of the form

$$\exp\left\{2\mu(E)\rho(t - t_{\text{eff}}(\theta))/\cos(\theta)\right\} \qquad (4)$$

Table 3
Effective thickness of the hexel aluminum plate for angles from 0° to 60° in 5° increments.

Angle (θ)	ρt (g/cm^2)	Error
0	0.2064	0.0029
5	0.2140	0.0048
10	0.2194	0.0046
15	0.2265	0.0047
20	0.2273	0.0059
25	0.2273	0.0045
30	0.2286	0.0038
35	0.2290	0.0055
40	0.2310	0.0053
45	0.2314	0.0034
50	0.2329	0.0029
55	0.2306	0.0067
60	0.2305	0.0049

where the factor of 2 accounts for both plates sandwiching the CPD. Also, $\rho t_{\text{eff}}(\theta)$ is the angular dependent effective thickness of the hexel aluminum plates interpolated from values in Table 3; $\mu(E)$ is the energy-dependent attenuation coefficient for aluminum; and $\rho t (= 0.23\,\text{g/cm}^2)$ is the hexel thickness assumed in the original model. The ρt term in the exponent removes the attenuation originally programmed into the response matrix and the $\rho t_{\text{eff}}(\theta)$ accounts more correctly for this effect.

Fig. 7 shows the Crab Nebula data [7] from Fig. 2 along with the results (dashed curve) of the correction for the hexel aluminum plates. The original model calculation (dotted curve) is shown for comparison. It can be seen from Fig. 7 that the dashed curve, in comparison to the measured count rates for the Crab in channel 1 (∼20–30 keV), better predicts the more forward-pointed angular distribution of the actual data than does the original response (dotted curve). The experimentally determined correction for the entrance window, as expected, contributes the largest improvement in predicting the trend of the lowest energy data below 60 keV, and near normal incidence to the detector. However, Fig. 7 also
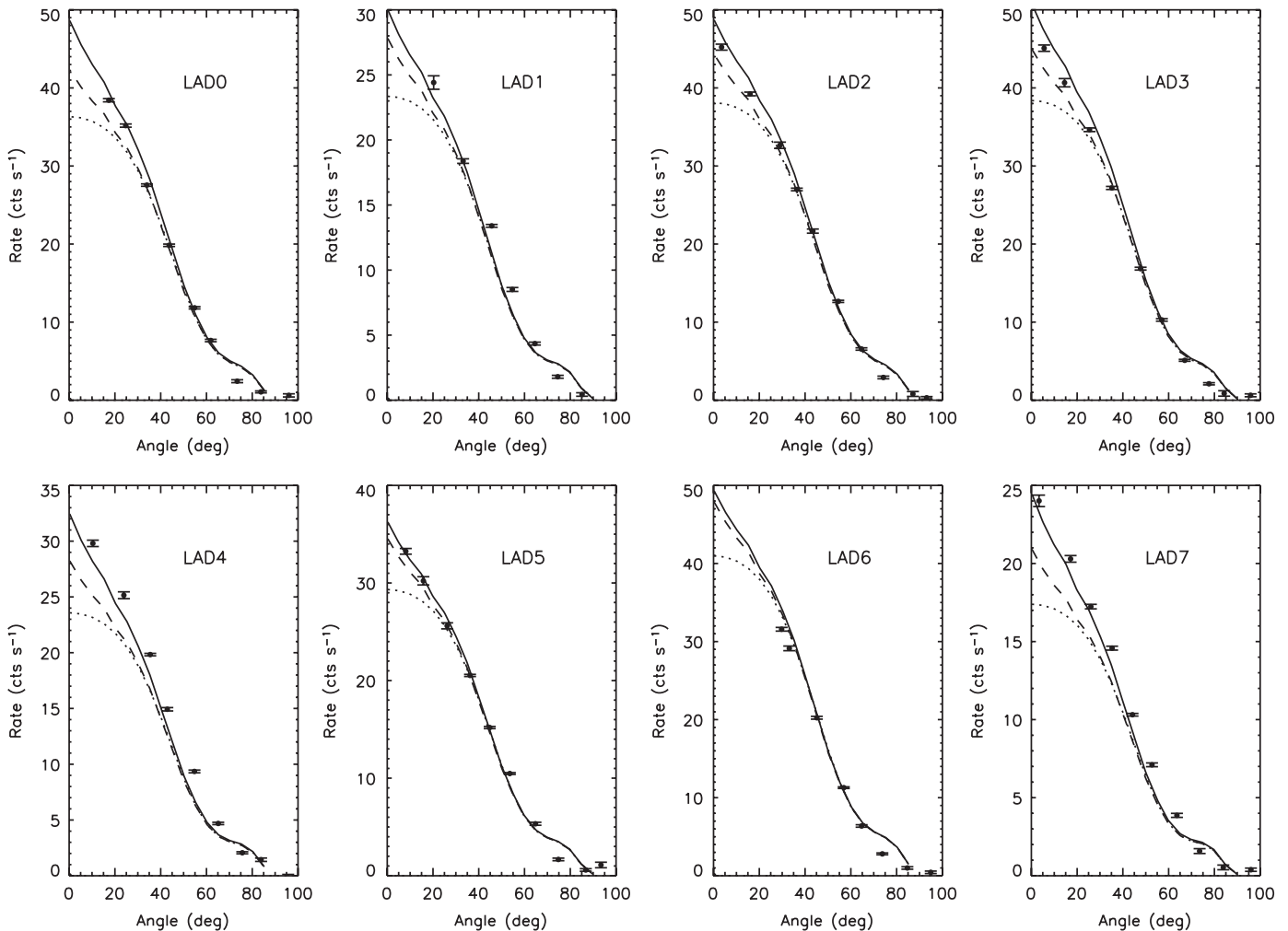

Fig. 7. Angular distribution of Crab Nebula Radiation for channel 1 of all LADs (as in Fig. 2). The data are shown with the original detector response (dotted line), the response corrected for the Hexel aluminum plates (dashed lines) and the response including all corrections (solid line).

Table 4
Detector dependent empirical effective area correction factors

LAD	Correction factor (A)
0	0.15
1	0.08
2	0.10
3	0.13
4	0.15
5	0.05
6	0.03
7	0.17

shows that, where Crab data were available at close to normal incidence (not available for LAD 6), the attenuation-corrected response is not completely successful in predicting the trend of the data. For some detectors and energy channels, the entrance window correction to the response model yielded only about 50% of the needed correction to fit the measured Crab flux. We investigated this further and found, in comparisons at all energies where the measured Crab data of sufficient statistical accuracy were available ($\sim$20–350 keV, see Fig. 13 of Harmon et al. [7] for channel 3), that there remained an unpredicted forward angle component in the data that was not reproduced by the combined original model + entrance window correction. Because of the energy range where this effect was seen, it was unlikely that any other source of photoelectric absorption, such as thermal blankets, would produce a significant effect that we have not modeled. We instead attributed this to the exclusion of data below 50 keV and to the assumed, relatively non-physical form of the angular distribution used to interpolate the Monte Carlo simulations at selected angles, which, as previously mentioned, was parameterized as a third-order polynomial of the cosine of the square of the incident angle [4]. Again, this provided an adequate representation for locating GRBs in combinations of 2, 3, or 4 LAD detectors at larger incident angles [6], but the assumed angular distribution did not match the more-sharply forward angle response seen in the measured Crab data.

Therefore, in addition to the entrance window correction, an additional energy-independent empirical correction was applied with the multiplicative form

$$1 + A \exp(-B\theta). \qquad (5)$$

The constant A was determined by matching the model and data in Fig. 7 for each LAD at $\theta = 0$. Values for A are listed in Table 4. The constant B, which described the correction for the forward angle effect, was found to have the same value 0.02 for each LAD. As with the attenuation correction, the input energy side of the BATSE detector response matrix was multiplied by this correction before

any spectral fitting. The application of this additional correction to response function applied to the Crab data is shown by the solid curve in Fig. 7. These two corrections greatly improve the response model for the LAD detectors.

4. Conclusion

As shown by Harmon et al. [7], the application of the corrections for the entrance window attenuation and for the empirically determined angular response at forward angles resulted in average daily measurements of the Crab Nebula flux that were more symmetric, less scattered and less skewed toward higher fluxes. These observations were verified independently in fitting Crab Nebula spectra data in individual LADs and comparing the results to those fit with the original matrix formalism. All measured parameters, such as the total flux, photon spectral indices, and quality of fit showed less variation from one detector to another and the overall scatter for measurements at different incident angles became more characteristic of Poisson-distributed data [7]. Although systematic errors remain, this general improvement in the ability to obtain more accurate flux information gave much better confidence in the use of BATSE Earth occultation data. These corrections were used in comparison of Crab Nebula data to measurements of the same source with those of other high-energy astronomy satellites [7], and were also globally applied to all of the BATSE Earth Occultation measurements in a catalog of 179 sources tabulated by Harmon et al. [11].

Acknowlegment

References

[1] W.C. Priedhorsky, et al., Astrophys. J. 280 (1984) 661.
[2] B. Schwarzschild, Phys. Today, August 2005, p. 21.
[3] G.J. Fishman, et al., in: S.E. Woosley (Ed.), AIP Conference Proceedings, vol. 115, High Energy Transients in Astrophysics, AIP, New York, p. 651.
[4] G.N. Pendleton, et al., Nucl. Instr. and Meth. A A 364 (1995) 567.
[5] G.N. Pendleton, Astrophys. J. 512 (1999) 362.
[6] G.N. Pendleton, et al., in: C. Fichtel, N. Gehrels, J. Norris (Eds.), Proceedings of the Second Compton Gamma-Ray Symposium, American Institute of Physics, 1994.
[7] B.A. Harmon, et al., Astrophys. J. Suppl. Ser. 138 (2002) 149.
[8] G.V. Jung, Astrophys. J. 338 (1989) 972.
[9] G.N. Pendleton, private communication.
[10] E. Storm, H.I. Israel, Nucl. Data Tables A 7 (1970) 565.
[11] B.A. Harmon, et al., Astrophys. J. 154 (2004) 585.